

Application of a Generalized RANS Wall Function to Recirculating Flows with Heat Transfer

T. J. Craft, S. E. Gant* & H. Iacovides

School of Mechanical, Aerospace and Civil Engineering, University of Manchester
 Sackville Street, PO Box 88, Manchester, M60 1QD, UK

*Correspondence author: Fax: +44 161 306 3723 Email: simon.gant@manchester.ac.uk

ABSTRACT

Despite the year-on-year increase in computer speeds, wall functions are still used in the majority of industrial turbulent flow CFD calculations. Their continued usage is driven by the desire to tackle new, larger, more complex, perhaps multiphysics, problems rather than simply improve upon the wall resolution of existing calculations. Whilst this desire is understandable, care should be taken in applying standard log-law wall functions to these complex flows. The present paper highlights the limitations of standard wall functions in predicting heat transfer downstream from a pipe expansion. An alternative *generalized* wall function is shown to give much improved results, comparable, in fact, to full low-Reynolds-number model treatments where a fine grid is used to resolve the viscous-affected sublayer. This new wall function has previously been applied to a range of flows, including fully-developed channel, impinging jet and spinning-disc flows. The present paper extends its application to flows involving corner-induced separations.

NOMENCLATURE

c_h, E	Constants of integration
k	Turbulent kinetic energy
y^+	Dimensionless wall distance, $y^+ = U_\tau y / \nu$
y^*	Dimensionless wall distance, $y^* = k^{1/2} y / \nu$
P_k	Production rate of k
T_τ	“Friction” temperature, $T_\tau = q_{wall} / \rho c_p U_\tau$
T^+	Dimensionless temperature, $T^+ = (T_{wall} - T) / T_\tau$
U_τ	“Friction” velocity, $U_\tau = \sqrt{\tau_{wall} / \rho}$
U^+	Dimensionless velocity, U / U_τ
ϵ	Dissipation rate

σ	Prandtl number
σ_t	Turbulent Prandtl number
κ	Von Kármán constant in the velocity log-law, $\kappa \approx 0.42$
κ_h	Von Kármán constant in the temperature log-law, $\kappa_h = \kappa / \sigma_t$
τ_{wall}	Wall shear stress

INTRODUCTION

The prediction of heat transfer downstream from an axisymmetric pipe expansion, and its 2D equivalent, the backward-facing step, has been the subject of numerous previous studies (e.g. [1, 2, 3, 4, 5]). This reflects both the usefulness of the flow for turbulence model validation and its industrial relevance. The flow involves a fully-developed pipe flow entering a larger-section pipe, whereupon the boundary layer separates at the sharp corner, undergoes flow curvature and then reattaches on the downstream pipe wall (see Figures 1 and 2 for a flow schematic and typical mean streamlines). Previous work within our research group has indicated that the use of standard linear eddy-viscosity RANS models is somewhat questionable in this flow, due to the linear model’s relatively poor performance in flows involving streamline curvature and flow impingement. The non-linear $k - \epsilon$ model of Craft *et al.* [6] is thus tested in the present paper, although linear $k - \epsilon$ model results are also shown for comparison. Since there are significant transport effects on the near-wall turbulence, standard wall functions are not generally accurate in such a flow. However, the alternative of fully-resolving the boundary layers, using low-Reynolds-number turbulence models, can lead to prolonged computing times. This is especially true if structured Cartesian meshes are employed, due to the fact that the fine grid near the walls extends into the main flow

domain. Although this latter problem could be alleviated, to some extent, by using hanging nodes or unstructured meshes to refine just the near-wall region, computing times would still be relatively large. An alternative approach, explored here, is to use a wall function that can accurately approximate the near-wall turbulence transport. As will be shown, this numerical wall-function approach offers significant savings in terms of computing times over the standard low-Reynolds-number model approach, whilst providing a comparable level of accuracy.

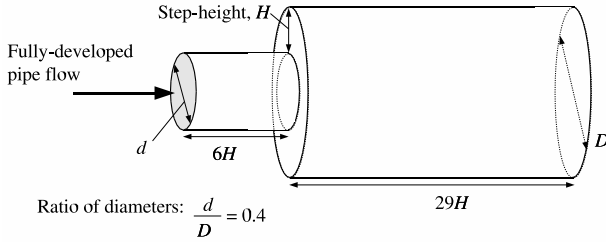


Figure 1: Pipe-expansion geometry

Results are shown for two Reynolds numbers: 17,000 and 40,000 (based on the downstream pipe diameter and bulk velocity). The ratio of the upstream to downstream pipe diameters, d/D , is 0.4. Experimental measurements of this configuration were undertaken by Yap [7]. Constant heat flux conditions are applied at the walls and the temperature differences are sufficiently small that variations of viscosity and density can be assumed negligible.

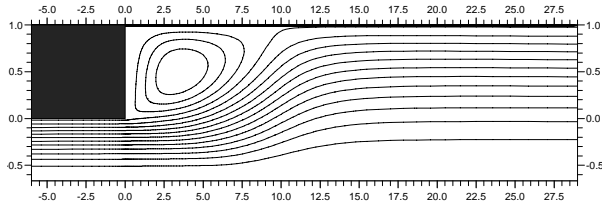


Figure 2: Typical calculated mean streamlines

NUMERICAL METHODS

Calculations were performed using the in-house finite-volume TEAM code [8]. This has a fully-staggered Cartesian grid arrangement where scalars are stored at cell centres and velocities at cell faces. The pressure-velocity coupling is handled by the SIMPLE algorithm, the third-order accurate QUICK scheme is used for convection of momentum and

temperature whilst power-law differencing (PLDS) is used for convection of turbulence parameters.

Two different RANS models are considered: the Launder-Sharma linear $k - \epsilon$ model [9] and the cubic non-linear $k - \epsilon$ model of Craft *et al.* [6]. The former model incorporates the so-called ‘‘Yap correction’’ [7], whilst the latter model uses a differential length-scale correction in addition to quadratic and cubic strain-rate/vorticity terms in the Reynolds-stress constitutive equation, and a strain-rate-dependent c_μ function (for details, see [5]). These two turbulence models are used in combination with three different wall treatments: a simplified form of the Chieng & Launder wall function [10] (hereafter denoted SCL), the generalized numerical wall function of Craft *et al.* [11] (denoted NWF) and low-Reynolds-number model treatments (denoted Low-*Re*). The SCL wall function is similar to the standard wall functions employed in many commercial CFD codes, with assumed logarithmic profiles for velocity and temperature:

$$U^* = \frac{1}{\kappa} \ln(Ey^*)$$

$$T^* = \frac{1}{\kappa_h} \ln y^* + c_h$$

In the above equations, the superscript ‘‘*’’ is used instead of the usual ‘‘+’’ to indicate that the velocity is made dimensionless with $k^{1/2}$ instead of $U_\tau = \sqrt{\tau_{wall}/\rho}$, following Launder & Spalding [12]. This avoids a singularity occurring at stagnation points, where τ_{wall} tends to zero. Cell-averaged production and dissipation rates are calculated for the k -equation by assuming constant values of shear stress and turbulence energy across the near-wall cell. The value of ϵ is specified at the wall-adjacent node based on the assumption of a linear length-scale variation ($l_m = \kappa y$). If the near-wall node is judged to be within the viscous sublayer (assumed to be $y^* < 21$) linear profiles are used for velocity and temperature ($U^* = y^*$ and $T^* = \sigma y^*$) instead of the log-laws, and the cell-averaged production is set to zero, $\overline{P}_k = 0$.

Numerical Wall Function: Details of the numerical wall function can be found in reference [11] and the PhD thesis of Gant [13]. Briefly, the model solves numerically the thin boundary-layer-type equations for wall-parallel momentum, k , $\tilde{\epsilon}$ and temperature across a fine grid embedded in the near-wall cells. The wall function transport equations take the generic form in Cartesian coordinates:

$$\rho U \frac{\partial \phi}{\partial x} + \rho V \frac{\partial \phi}{\partial y} = \frac{\partial}{\partial y} \left(\Gamma \frac{\partial \phi}{\partial y} \right) + S$$

where ϕ denotes U , k , $\bar{\epsilon}$ or T , the y -direction is normal to the wall and the source term S includes the pressure-gradient in the momentum equation and the production and dissipation terms in the k and $\bar{\epsilon}$ equations. For the present application, cylindrical-polar coordinates are used for the embedded-grid transport equations. Instead of solving a pressure-correction equation across the embedded grid, the wall-normal velocity is calculated from continuity. One iteration of the wall-function calculations is performed for each main-grid iteration, so the solutions in the near-wall region and in the bulk of the flow domain converge at the same time. Following each iteration, the near-wall profiles of U , k , $\bar{\epsilon}$ and T are used to calculate wall-function parameters, such as the wall shear stress, τ_{wall} , cell-averaged production and dissipation rates, \overline{P}_k and $\bar{\epsilon}$, and wall heat flux, q_{wall} . These wall-function parameters are then employed as boundary conditions and modified source terms in the main-grid code in much the same way as with standard log-law wall functions. Previous studies [11, 13] have shown that this wall function produces results in good agreement with full low-Reynolds-number model treatments in flows with a single plane wall (channel flow, impinging jets and spinning discs). For the present flow, additional consideration needs to be given to the treatment of corners.

At external (i.e. convex) corners, within the embedded-grid zone, zero gradient conditions in the wall-parallel direction are used to specify U , V , k , $\bar{\epsilon}$ and T on the open-end boundary (see Figure 5). This zero-gradient condition has, in fact, little effect on the solution, since in any case wall-parallel gradients in the diffusion term are ignored in the wall-function region ($\partial/\partial x (\Gamma \partial \phi / \partial x)$ is assumed zero). It was also found necessary to set the pressure gradient in the wall-function domain to zero for two rows of cells adjacent to the external corner. This ad-hoc correction was necessary to prevent an unphysical flow reversal in the near-wall region. However, even without the the correction the flow reversal was limited to just a few cells and produced only a minor difference in the overall heat transfer predictions.

For internal corners, there are effectively two overlapping numerical wall function calculations for the same main-grid cell in the corner (when the wall-function is applied separately to the north and the west faces of the corner cell). To calculate the cell-averaged source terms for the main-grid k and $\bar{\epsilon}$ equations in this cell, the arithmetic mean is taken of the the two wall-function values. For example, if the cell-averaged production calculated from applying the wall-function to the north face of the cell is \overline{P}_k^{north} ,

and to the west face, \overline{P}_k^{west} , then the value used in the main-grid calculation is just $0.5 \left(\overline{P}_k^{north} + \overline{P}_k^{west} \right)$. A similar approach is used for the cell-averaged dissipation, ϵ , wall damping, E , and Yap correction, Y_c . In fact, tests have shown that the overall predicted flow is reasonably insensitive to the treatment of these corner cells.

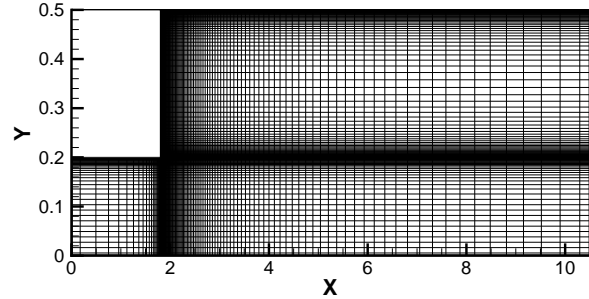


Figure 3: Low- Re grid 140×140

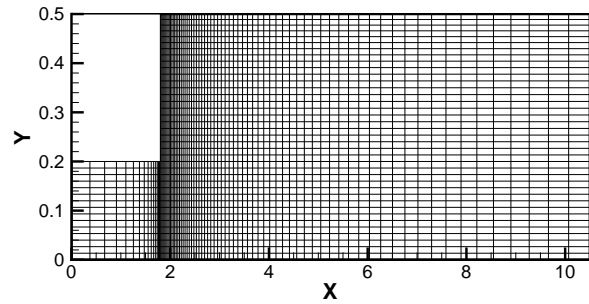


Figure 4: Wall-function grid 85×40

Computational Grids: For the low-Reynolds-number model, a grid of 140×140 nodes was used (Figure 3) which for the higher Reynolds number gave $y^+ < 1$ on all walls except for a few nodes near the external corner on the downstream-facing step. Increasing the number of nodes to 160×160 had practically no effect on the predicted heat transfer coefficient, whilst reducing the number of nodes to 102×120 (axial \times radial) did produce a moderate change. Results using the 140×140 grid were therefore considered adequately grid-independent. For the wall-function calculations, three different grids were employed, using 85×50 , 85×40 and 85×30 nodes in the axial \times radial directions, respectively (see, for example, Figure 4). The near-wall cell

size with the coarsest 85×30 grid was approximately double that of the finest 85×50 grid (a maximum y^+ of 48 compared to $y_{max}^+ = 23$ for the 85×50 grid). Figure 5 shows a close-up view of the external corner with the embedded grid. For the 85×50 grid, 30 additional nodes were used on each wall in the embedded grid, whilst for the coarser 85×40 and 85×30 grids 40 embedded grid nodes were used. Using greater grid resolution in the wall-function domains made no difference to the results.

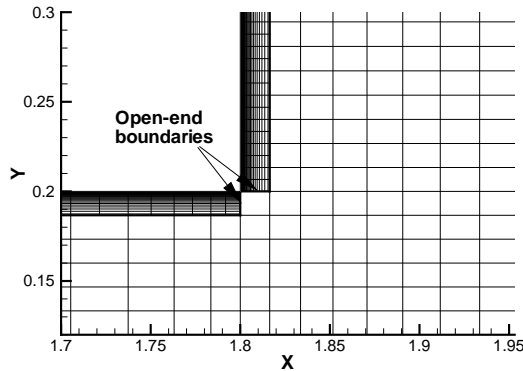


Figure 5: Close-up of the external corner region showing the embedded grid used with the numerical wall function.

RESULTS

The predicted Nusselt numbers on the downstream (outer) pipe wall using the linear $k - \epsilon$ model at $Re = 40,000$ are shown in Figures 6a and 6b. The two plots compare the results of the SCL and NWF wall-function treatments using three different grids against those of the low-Reynolds-number model and the experimental data of Yap [7]. In these, and subsequent figures, the Nusselt number is normalized with the Nusselt number of fully-developed pipe flow, $Nu_{DB} = 0.023Re^{0.8}Pr^{0.4}$. The low- Re linear $k - \epsilon$ model is in fairly good agreement with the overall shape of the experimental Nu distribution, although the peak value is over-predicted by around 20%. By comparison, the standard SCL wall function underpredicts the experimental Nu by around 40% and the peak value occurs too far upstream, at approx. $x/H \approx 6$ instead of the experimental peak plateau between $8 \leq x/H \leq 10$. There is a sudden change in the slope of the SCL wall function Nu profile using the 85×50 grid in the recovery region at $x/H \approx 17$. This is due to the viscous sublayer becoming sufficiently thick that the near-wall y^* drops below the threshold value of 21 and the wall function therefore selects linear velocity and temperature profiles instead of the log-law.

In contrast to the SCL results, the numerical wall function results (Figure 6b) are in good agreement with those of the low- Re model, both in terms of shape and peak values of Nu . There is a mild dependence on the near-wall cell size in the region of flow separation, from $x/H = 0$ to $x/H = 10$, with the Nu peak becoming somewhat overpredicted and moving upstream as the number of grid nodes is reduced from 85×50 to 85×30 . This grid dependence, although fairly small, is slightly greater than that observed previously in applying the NWF to impinging jet flows (see [11]).

The non-linear $k - \epsilon$ model results in Figures 7a and 7b show broadly similar trends to those observed with the linear model. Overall, the Nusselt number levels are slightly lower using the non-linear model, with the low- Re model overpredicting the experimental values by only around 5%, whilst the location of the peak Nu occurs at around $3H$ too far downstream. The SCL wall function results, again, significantly underpredict the heat transfer coefficient whilst the numerical wall function shows good agreement with the low- Re model, with a similar level of grid dependence to that exhibited previously with the linear model.

Corresponding results at the lower Reynolds number of $Re = 17,000$ are shown in Figure 8 for the linear $k - \epsilon$ model and Figure 9 for the non-linear model. The SCL and NWF show similar trends to those exhibited at the higher Reynolds number. Interestingly, the linear $k - \epsilon$ model actually performs better here than the non-linear model. It should be noted that this Reynolds-number-sensitivity of the Craft *et al.* non-linear model is currently being investigated by the Manchester University (ex-UMIST) group.

A comparison of the computing times for the three different wall treatments is given in Table 1. The numerical wall function calculation took approximately twice as long as the log-law SCL wall function calculation but was a staggering 260 times faster than the full low-Reynolds-number model calculation. All calculations were performed using the same levels of compiler optimization and under-relaxation on an Intel P4 2.8GHz desktop PC.

CONCLUSIONS

The generalized numerical wall function of Craft *et al.* [11] has been applied to a pipe-expansion flow at two Reynolds numbers, using two different turbulence models. Results obtained using this numerical wall function are in very good agreement with the Nusselt number predictions of the full low-Reynolds-number model treatments and experimental data. In

contrast, the standard log-law wall function is unable to capture the correct heat transfer trends and the results are sensitive to the location of the edge of the viscous sublayer. Computing times are two orders of magnitude less with the numerical wall function than the full low- Re treatment.

The numerical wall function clearly offers the benefits of an accuracy comparable to the low- Re approach at a vastly reduced computing cost. The speed advantages of the wall function are due to two principal factors: a considerably lower number of grid cells and a faster solution methodology based on solving parabolic-type transport equations in the near-wall region and using continuity instead of a pressure-correction equation to determine the wall-normal velocity. The comparisons of computing times shown here are based on the use of a structured Cartesian grid, which inevitably leads to the low- Re approach being extremely costly due to the fine grid cells extending from the wall-region into the main flow domain. However, one would still expect the low- Re model calculations to take considerably longer than those of the numerical wall-function even if unstructured locally-refined grids had been used.

ACKNOWLEDGMENTS

Authors' names appear alphabetically.

REFERENCES

- [1] S. H. Ko. Computation of turbulent flows over backward and forward-facing steps using a near-wall Reynolds stress model. In *Annual Research Briefs 1993*, Center for Turbulence Research, Stanford University, 1993.
- [2] W. C. Lasher and D. B. Taulbee. Calculation of turbulent backstep flow: commentary on modelling of the pressure-strain correlation. In W. Rodi and S. Ganic, editors, *Engineering Turbulence Modelling and Experiments*. Elsevier, 1990.
- [3] H. Le and P. Moin. Direct numerical simulation of turbulent flow over a backward-facing step. In *Annual Research Briefs 1992*, Center for Turbulence Research, Stanford University, 1992.
- [4] W. Cabot. Near-wall models in large eddy simulations of flow behind a backward-facing step. *Center for Turbulence Research, Annual Research Briefs*, 1996.
- [5] T. J. Craft, H. Iacovides, and J. H. Yoon. Progress in the use of non-linear two-equation models in the computation of convective heat-transfer in impinging and separated flows. *Flow, Turbulence and Combustion*, 63:59–80, 1999.
- [6] T. J. Craft, B. E. Launder, and K. Suga. Development and application of a cubic eddy-viscosity model of turbulence. *Int. J. Heat and Fluid Flow*, 17:108–115, 1996.
- [7] C.R. Yap. *Turbulent heat and momentum transfer in recirculating and impinging flows*. PhD thesis, Dept. of Mechanical Engineering, Faculty of Technology, University of Manchester, 1987.
- [8] P.G. Huang and M.A. Leschziner. *TEAM, an introduction and guide to the computer code*. Dept. of Mechanical Engineering, Faculty of Technology, University of Manchester, 1984.
- [9] B. E. Launder and B. I. Sharma. Application of the energy-dissipation model of turbulence to the calculation of flow near a spinning disc. *Lett. in Heat Mass Transfer*, 1:131–138, 1974.
- [10] C. C. Chieng and B. E. Launder. On the calculation of turbulent heat transport downstream from an abrupt pipe expansion. *Numerical Heat Transfer*, 3:189–207, 1980.
- [11] T. J. Craft, S. E. Gant, H. Iacovides, and B. E. Launder. A new wall function strategy for complex turbulent flows. *Numerical Heat Transfer, Part B: Fundamentals*, 45(4):301–318, 2004.
- [12] B. E. Launder and D. B. Spalding. The numerical computation of turbulent flows. *Computer Methods in Applied Mechanics and Engineering*, 3:269–289, 1974.
- [13] S. E. Gant. *Development and application of a new wall function for complex turbulent flows*. PhD thesis, University of Manchester Institute of Science and Technology, 2002. (Download from <http://cfcd.me.umist.ac.uk>).

Wall Treatment	Grid Nodes	Iterations	CPU Time (s) per iteration	Total CPU Time (s)	Relative Time
SCL	85 × 50	13125	0.0072	95	1
NWF	85 × 50	11484	0.0160	184	1.94
Low- Re	140 × 140	754720	0.0643	48540	510

Table 1: Comparison of computing times for the linear $k - \epsilon$ model at $Re = 40,000$. For the numerical wall function, 30 additional embedded-grid nodes were used along each of the three wall sections.

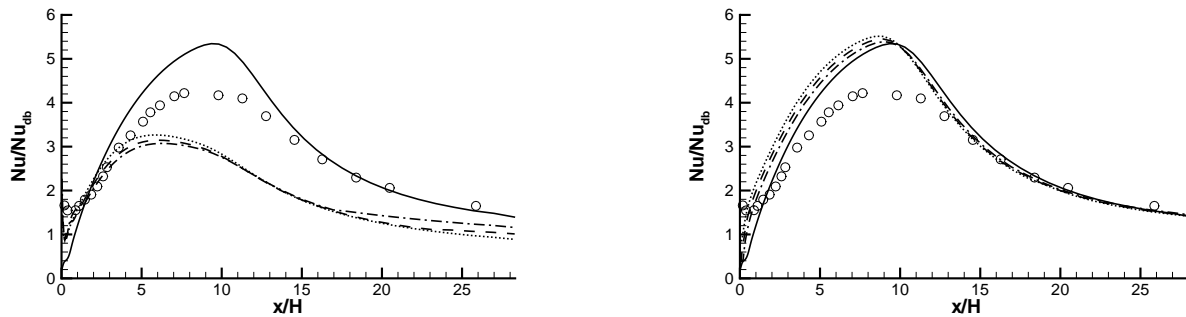


Figure 6: $Re = 40,000$ using the linear $k - \epsilon$ model

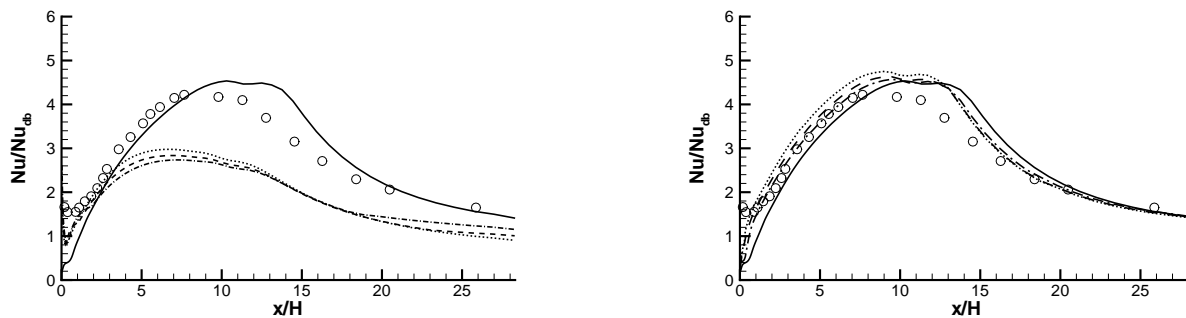


Figure 7: $Re = 40,000$ using the non-linear $k - \epsilon$ model

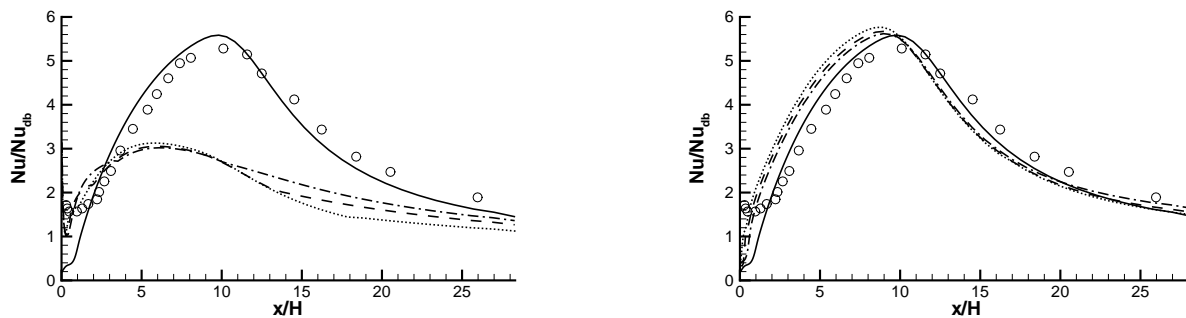


Figure 8: $Re = 17,000$ using the linear $k - \epsilon$ model

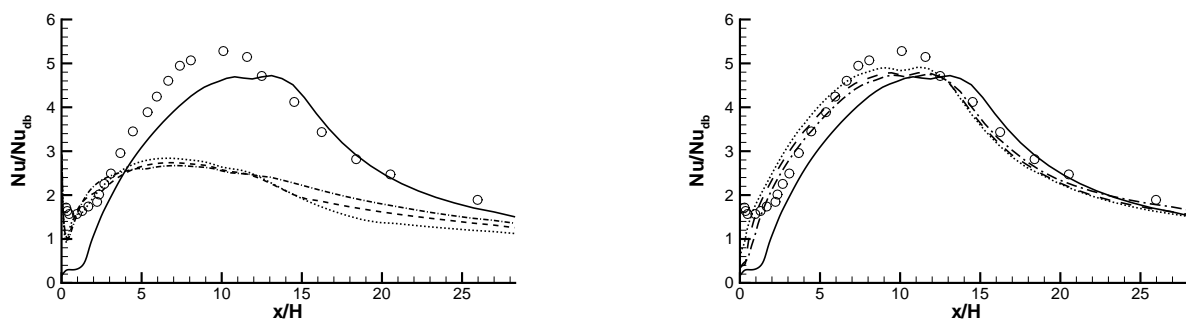


Figure 9: $Re = 17,000$ using the non-linear $k - \epsilon$ model

The graphs on this page present Nusselt number profiles on the downstream pipe wall. Those on the left-hand-side of the page are SCL wall function results and on the right are NWF results. Solid line: low- Re model results; broken lines: wall function calculations using different grids (\cdots : 85×30 ; $---$: 85×40 ; $- \cdot -$: 85×50), symbols: experiments.